GEOPHYSICS, VOL. 75, NO. 1 (JANUARY-FEBRUARY 2010); P. N19–N31, 6 FIGS., 2 TABLES.
10.1190/1.3279833

Stochastic joint inversion of 2D seismic and seismoelectric signals in linear poroelastic materials: A numerical investigation

Abderrahim Jardani[2], André Revil[1,3], Evert Slob[1,4], and Walter Söllner[5]

ABSTRACT

The interpretation of seismoelectrical signals is a difficult task because coseismic and seismoelectric converted signals are recorded simultaneously and the seismoelectric conversions are typically several orders of magnitude smaller than the coseismic electrical signals. The seismic and seismoelectric signals are modeled using a finite-element code with perfectly matched layer boundary conditions assuming a linear poroelastic body. We present a stochastic joint inversion of the seismic and seismoelectrical data based on the adaptive Metropolis algorithm, to obtain the posterior probability density functions of the material properties of each geologic unit. This includes the permeability, porosity, electrical conductivity, bulk modulus of the dry porous frame, bulk modulus of the fluid, bulk modulus of the solid phase, and shear modulus of the formations. A test of this approach is performed with a synthetic model comprising two horizontal layers and a reservoir partially saturated with oil, which is embedded in the second layer. The result of the joint inversion shows that we can invert the permeability of the reservoir and its mechanical properties.

INTRODUCTION

The electroseismic (electric-to-seismic) and seismoelectric (seismic-to-electric) phenomena correspond to coupling between electromagnetic disturbances and seismic disturbances in a porous material (Frenkel, 1944; Pride, 1994). Any mineral in contact with water is the setting of electrochemical reactions at its surface. A surface charge is formed, which is fixed in a Lagrangian framework attached to the solid phase. This charge is shielded partly by the sorption of counterions in the Stern layer coating the surface of the minerals (Stern, 1924; Revil and Leroy, 2001; Leroy and Revil, 2004). Global electroneutrality at the scale of a representative elementary volume requires an excess of electrical charges located in the vicinity of the mineral/water interface, in the so-called electrical diffuse layer (Bokris and Reddy, 1970; Pride, 1994). The diffuse and Stern layers form the electrical double layer. The Stern layer is part of the total fixed charge attached to the solid phase, whereas the diffuse layer can be dragged by the flow of the pore water relative to the mineral framework. The electroseismic and seismoelectric couplings are controlled by the relative displacement between the charged solid phase (with the Stern layer attached to it) and pore water (with its diffuse layer and consequently an excess of electrical charges per unit pore volume).

In this paper, we are interested only in the seismoelectric coupling corresponding to electromagnetic conversion of mechanical energy during the propagation of seismic waves in poroelastic media. We want to know how the coupled seismic and seismoelectric information can be used, for instance, to determine the permeability of an oil reservoir. The same type of methodology could be applied to image nonaqueous phase liquid (NAPL)/dense nonaqueous phase liquid (DNAPL) plumes for shallow groundwater remediation problems. When seismic waves propagate in a linear poroelastic porous material, two types of electrical disturbances are observed. The propagation of seismic waves (P- and S-waves) generates an electrical current associated with the displacement of the electrical diffuse layer in a Lagrangian framework attached to the solid phase. These coseismic electrical signals travel at the same speed as the seismic waves (Pride, 1994). The amplitudes of the coseismic electromagnetic signals are controlled by the properties of the porous material (the formation factor) and by the properties of the pore fluid/solid interface (the zeta potential in the theory of Pride [1994] the excess charge per unit pore volume in the formulation developed by Revil et al. [2003] and Revil [2007]).

Manuscript received by the Editor 7 March 2009; revised manuscript received 21 July 2009; published online 25 January 2010.
[1]Colorado School of Mines, Department of Geophysics, Golden, Colorado, U.S.A. E-mail: arevil@mines.edu.
[2]Formerly Colorado School of Mines, Department of Geophysics, Golden, Colorado, U.S.A.; presently Université de Rouen, Morphodynamique Continentale et Côtière, Mont Saint Aignan, France. E-mail: ajardani@mines.edu.
[3]Université de Savoie, INSU-CNRS LGIT, Le Bourget du Lac, France. E-mail: arevil@mines.edu.
[4]Delft University of Technology, Department of Geotechnology, Delft, The Netherlands. E-mail: e.c.slob@tudelft.nl.
[5]Petroleum Geo-Services, Lysaker, Norway. E-mail: walter.sollner@pgs.com.

In addition to the coseismic signals, another phenomenon occurs when a seismic wave moves through a sharp interface characterized by a change in the textural properties or a change in salinity or clay content/mineralogy. In this situation, a fraction of the mechanical energy is converted into electromagnetic energy and a dipolar electromagnetic excitation is produced. The resulting electromagnetic disturbances diffuse very quickly through the geologic strata and can be recorded, nearly instantaneously, by electrodes or antennas located at the ground surface, in boreholes (Mikhailov et al., 1997; Butler et al., 1997), or at the seafloor, for instance. This seismoelectric conversion can be used as a tool to diagnose and locate oil reservoirs because this information can be used in principle to determine remotely their permeability and electrical conductivity (hence possibly the saturation of oil in the reservoir) as shown below.

Thompson and Gist (1993) present a case study for the exploration of oil and gas using seismoelectric converted electrical signals. They used adapted data processing and common midpoint (CMP) techniques to produce a seismoelectric image of the subsurface to depths on the order of a few hundred meters. They concluded that seismoelectric conversions could be detected from a depth of 300 m. Thompson et al. (2007) suggest that these methods could be used for much greater depths (several kilometers in the case of the electroseismic method). The seismoelectric method also has been used for a variety of applications in near-surface geophysics (Migunov and Kokorev, 1977; Fourie, 2003; Kulessa et al., 2006). Mikailov et al. (2000) describe crosshole seismoelectric measurements in a small-scale laboratory experiment with vertical and inclined fractures located between the source and receivers. They recorded not only the coseismic electric signals generated by the seismic wave arriving at the receivers, but also the EM-wave associated with the Stoneley wave excited in the fracture. They claimed a tomography image with traveltimes extracted from the seismoelectric measurements possibly could be constructed. Other studies, such as Block and Harris (2006), have been focused to understand the influence of the salinity on the magnitude of the coseismic signals.

The model developed by Pride (1994) couples Biot's theory to the Maxwell equations via a source current density of electrokinetic origin. A sensitivity analysis of this model can be found in Haartsen et al. (1998). This model has opened the door to numerical modeling of the coseismic and seismoelectric conversions using finite-difference or finite-element methods and to assess the usefulness of these methods for application to the field (Butler et al., 1997; Haartsen and Pride, 1997; Garambois and Dietrich, 2002; Dupuis et al., 2007; Haines et al., 2007; Strahser et al., 2007). Haines and Pride (2006) use a finite-difference algorithm to simulate the 2D seismoelectric response of a heterogeneous medium taking into account all the poroelastic waves modes (fast waves, slow waves, and shear waves) and their coseismic electrical signals plus the seismoelectric conversions. They were interested by the possibility to use the seismoelectric method for shallow seismoelectric investigations (tens to hundreds of meters) using a frequency range from 10 Hz to 1 kHz. Their algorithm can be used to obtain an idea about the sensitivity of the seismoelectric signal with respect to the reservoir geometry. Pain et al. (2005) present a 2D mixed finite-element algorithm to solve the poroelastic Biot equations including the electrokinetic coupling to study the sensitivity of the seismoelectric method to material properties, such as porosity and permeability of geologic formations surrounding a borehole.

We propose below a methodology to invert the mechanical, transport, and electrical properties of a reservoir with an arbitrary geometry using a stochastic joint inversion of seismograms and seismoelectrograms (electrograms). The electrodes can be collocated with the geophones to facilitate the separation of the coseismic electrical signals from seismoelectric (converted) signals. The section entitled "Forward Problem" is focused on the description of the forward modeling using a finite-element code. The section entitled "Stochastic Joint Inversion" describes the stochastic algorithm used to perform the joint inversion. The section entitled "Application to a Synthetic Case Study" shows a validation of the algorithm to a synthetic case.

FORWARD PROBLEM

Wave equations in a poroelastic body

Biot's theory (Biot, 1956a and 1956b) provides a starting framework to model the propagation of seismic waves in linear poroelastic media. The theory predicts the existence of an additional compressional wave by comparison with the P- and S-waves found for elastic materials. The existence of this slow P-wave was first confirmed by Plona (1980). The physical interpretations of the elastic constants in Biot's theory are given by Biot and Willis (1957) and Geertsma and Smit (1961).

According to Biot's theory and neglecting the electro-osmotic contribution in the Darcy velocity, the equations of motion in a 2D statistically isotropic, fully saturated, heterogeneous, and porous elastic medium are given, in the frequency domain, by (e.g., Haartsen et al., 1998)

$$-\omega^2(\rho\mathbf{u} + \rho_f\mathbf{w}) = \nabla\cdot\mathbf{T} + \mathbf{F}, \tag{1}$$

$$\mathbf{T} = [\lambda_u\nabla\cdot\mathbf{u} + C\nabla\cdot\mathbf{w}]\mathbf{I} + G[\nabla\mathbf{u} + \nabla\mathbf{u}^T], \tag{2}$$

$$-\omega^2(\rho_f\mathbf{u} + \tilde{\rho}_f\mathbf{w}) - jb\omega\mathbf{w} = -\nabla p, \tag{3}$$

and

$$-p = C\nabla\cdot\mathbf{u} + M\nabla\cdot\mathbf{w} + \mathrm{S}, \tag{4}$$

where $j^2 = -1$, $\mathbf{u}$ is the averaged displacement vector of the solid, $\mathbf{w}$ is the averaged displacement vector of the fluid relative to the solid (called the filtration displacement), $\mathbf{T}$ is the stress tensor, $\mathbf{I}$ is the identity matrix, $\mathbf{F}$ is the body force on the elastic solid phase, $\mathbf{F}_f$ is the body force on the viscous fluid phase, S is a pressure source acting on the pore fluid, ρ represents the mass density of the saturated medium, ρ_f and ρ_s are the mass density of the fluid and the solid, respectively, $\tilde{\rho}_f$ is an apparent density of the pore fluid, p is the averaged fluid pressure, $\lambda_u = K_u - (2/3)G$ is the undrained Lamé modulus of the porous material, b is the mobility of the fluid, G is the shear modulus of the porous frame, and C and M are elastic moduli. A time dependence of $\exp(-j\omega t)$, with angular frequency ω, is assumed.

Equation 1 corresponds to Newton's law, whereas equation 2 represents a constitutive expression for the total stress tensor as a function of the displacement (Hooke's law). This constitutive equation comprises the classical term of linear elasticity plus an additional term related to the expansion/contraction of the porous body to accommodate the flow of the pore fluid relatively to a Lagrangian framework attached to the solid phase. Equation 3 is the Darcy con-

stitutive equation in which the bulk force acting on the fluid phase has been neglected and equation 4 is one of the classical Biot constitutive equations of poroelasticity. The mass density of the porous material is given as $\rho = \phi\rho_f + (1-\phi)\rho_s$.

The material properties entering equations 1–4 are given by Pride (1994) and Rañada Shaw et al. (2000),

$$b = \frac{\eta_f}{k_0}, \tag{5}$$

$$\tilde{\rho}_f = \frac{\rho_f \phi}{a}, \tag{6}$$

$$\alpha = 1 - K_{fr}/K_s \tag{7}$$

$$K_u = \frac{K_f(K_s - K_{fr}) + \phi K_{fr}(K_s - K_f)}{K_f(1 - \phi - K_{fr}/K_s) + \phi K_s}, \tag{8}$$

$$C = \frac{K_f(K_s - K_{fr})}{K_f(1 - \phi - K_{fr}/K_s) + \phi K_s}, \tag{9}$$

$$M = \frac{C}{\alpha} = \frac{K_f K_s}{K_f(1 - \phi - K_{fr}/K_s) + \phi K_s}, \tag{10}$$

where K_u (in Pa) is the (undrained) bulk modulus of the porous medium, K_{fr} is the bulk modulus of the dry porous frame (skeleton), K_f is the bulk modulus of the fluid, K_s is the bulk modulus of the solid phase, and α is the Biot-Willis coefficient. Equation 8 is the Gassman equation, η_f is the dynamic viscosity of the pore fluid, k_0 the permeability of the medium, ϕ the porosity, and a is the tortuosity. The ratio a/ϕ corresponds to the electrical formation factor F, also defined by Archie's law $F = \phi^{-m}$ where m is called the cementation exponent. In the following, we consider the tortuosity equal to $\phi^{-1/2}$, which is equivalent to take a cementation exponent equal to 1.5.

The classical formulation described above in equations 1–4 is based on solving partial differential equations for two unknown fields $\mathbf{u}$ and $\mathbf{w}$. For a 2D discretized problem, four degrees of freedom per node are therefore present. All the studies dealing with the modeling of the seismoelectric problem use this type of formulation (e.g., Haarsten and Pride, 1997; Haartsen et al., 1998; Garambois and Dietrich, 2002; Haines and Pride, 2006). Atalla et al. (1998) introduce an alternative approach using $\mathbf{u}$ and p as unknowns (see also Karpfinger et al., 2009). This implies three unknown parameters (u_1, u_2, and p) to solve at each node. After some algebraic manipulations described in Appendix A, the equations of motion can be written in terms of the two new unknown fields ($\mathbf{u}$, p) as

$$-\omega^2 \rho_\omega^s \mathbf{u} + \theta_\omega \nabla p = \nabla \cdot \hat{\mathbf{T}} + \mathbf{F}, \tag{11}$$

$$\hat{\mathbf{T}} = \lambda(\nabla \cdot \mathbf{u})\mathbf{I} + G[\nabla \mathbf{u} + \nabla \mathbf{u}^{\mathrm{T}}], \tag{12}$$

$$\mathbf{T} = \hat{\mathbf{T}} - \alpha p \mathbf{I}, \tag{13}$$

$$\frac{1}{M}(p + S) + \nabla \cdot \{k_\omega[\nabla p - \omega^2 \rho_f \mathbf{u}]\} = -\alpha \nabla \cdot \mathbf{u}. \tag{14}$$

Equation 11 corresponds to Newton's law applied to the solid skeleton of the porous material. This equation is similar to Newton's equation of elastic bodies except for the coupling term $\theta_w \nabla p$, which represents the coupling between the solid and fluid phases. The stress tensor defined by equation 12 corresponds to the stress tensor with the porous material in vacuum (i.e., it corresponds to the stress acting on the solid phase if the pore fluid is replaced by vacuum). Equation 13 describes the relationship between the total stress tensor and effective stress tensor. The material properties entering into equations 11–14 are given by

$$k_\omega = \frac{1}{\omega^2 \tilde{\rho}_f + j\omega b}, \tag{15}$$

$$\lambda = K - \frac{2}{3}G, \tag{16}$$

$$\rho_\omega^s = \rho - \omega^2 \rho_f^2 k_\omega, \text{ and} \tag{17}$$

$$\theta_\omega = \alpha - \omega^2 \rho_f k_\omega, \tag{18}$$

where k_ω is not the dynamic permeability of the porous material (the dynamic permeability is given in Appendix A), $\tilde{\rho}_f$ is an effective fluid density, λ is the Lamé coefficient, and ρ_ω^s corresponds to the apparent mass density of the solid phase at a given frequency ω.

Description of the seismic source

In the following example, we use a source generating P-waves only. This force creates a net force on the solid phase of the porous rock. Because the source generates a displacement of pore water relative to the grain framework, it creates an electromagnetic disturbance. This disturbance diffuses nearly instantaneously to all receivers and has quite a strong amplitude. Because this contribution can be removed easily from the electrograms, we will not model it below.

Using the Fourier transformation of the first time derivative of the Gaussian function for such a source yields the following expression for the bulk force acting on the solid phase

$$\mathbf{F}(x,y,\omega) = F(\omega)\nabla[\delta(x - x_0)\delta(y - y_0)], \tag{19}$$

$$F(\omega) = \mathrm{FT}[(t - t_0)\exp\{-[\pi f_0(t - t_0)]^2\}], \tag{20}$$

where $\mathrm{FT}[f(t)]$ is the Fourier transform of the function $f(t)$, t_0 is the time delay of the source, and f_0 is its dominant frequency. This force is a source term acting on the right-hand side of equation 11. In the following, we will neglect the pore fluid pressure source term S, which is equivalent to neglecting the electromagnetic effects associated with the seismic source itself. A complete analysis of the electromagnetic effects associated with elementary sources can be found in Pride and Haartsen (1996).

Description of the electrokinetic conversion

The electrokinetic coupling at work in the seismoelectric response is the result of the relative displacement of the pore water with respect to the solid phase. The drag of the charge density contained in the pore water is responsible for a net source current density in a framework attached to the solid phase (Revil et al., 1999; Leroy and Revil, 2004). The model developed by Pride (1994) is an extension of the classical streaming potential theory and takes the form of the Biot equations coupled to the Maxwell equations via the source current density. This formulation has a drawback of the required knowledge of the zeta potential, a microscopic potential of the electrical double layer at the pore water/solid interface. Recently, a new formulation of the streaming potential has been developed and tested on experimental, sandbox, and field data (see Bolève et al., 2007; Revil et al., 2007 and references therein). We use this alternative theory here, which has the advantage to require knowledge of only the permeability as shown below.

In addition, we consider below the electromagnetic disturbances in the quasi-static limit of the Maxwell equations as in the study of self-potential signals (Suski et al., 2006; Jardani et al., 2007). This assumption is valid because the target is assumed to be close enough (less than 1 km) from the receivers (antennas, nonpolarizing electrodes, and magnetometers). In such a case, we can neglect the time required by the electromagnetic disturbances to diffuse between the reservoir and receivers (see Revil et al. [2003] for a discussion of the diffusion time associated with the diffusion of low-frequency EM disturbances).

Using the model developed by Revil and Linde (2006) with the previous assumptions, we can model the problem by solving only the quasi-static Poisson-type problem

$$\nabla \cdot (\sigma \nabla \psi) = \nabla \cdot \mathbf{j}_S, \tag{21}$$

$$\mathbf{j}_S = \bar{Q}_V \dot{\mathbf{w}} = -j\omega \bar{Q}_V k_\omega (\nabla p - \omega^2 \rho_f \mathbf{u}), \tag{22}$$

where ψ is the electrostatic potential ($\mathbf{E} = -\nabla\psi$ in the quasi-static limit of the Maxwell equations), σ is the electrical conductivity of the medium, $\mathbf{j}_S$ is the source current density of electrokinetic nature, and $\bar{Q}_V$ is the excess of charge (of the diffuse layer) per unit pore volume (in C m^{-3}). For saturated rocks, $\bar{Q}_V$ can be computed directly from the DC permeability k_0 through a semiempirical formula derived by Jardani et al. (2007), which is valid for any type of texture and mineralogy. Therefore, we consider below that $\bar{Q}_V$ and k_0 are not independent parameters. The model proposed by Linde et al. (2007) and Revil et al. (2007) predict, that for a partially water-saturated reservoir, $\bar{Q}_V$ should be replaced by $\bar{Q}_V / S_W$ where S_W is the partial saturation in water.

Regarding the electric problem, we use PML boundary conditions keeping the same values for the damping coefficients α_{x_i}, σ_{x_i}, and k_{x_i} (see Appendix B). The reason for this choice is that the amplitude of the seismoelectric conversions in the PML layer is tied to the amplitude of the seismic waves. Therefore, the attenuation of the seismoelectric conversions is warranted by the attenuation of the seismic waves.

Regarding seismoelectric conversions, they are associated with drops in the value of the electrical conductivity and volumetric charge per unit volume. Because the porosity influences the electrical formation factor, hence the electrical conductivity, and because permeability is connected strongly to the volumetric charge per unit volume, the porosity and permeability also influence the existence of interfacial seismoelectric conversions. This implies, in turn, that the seismoelectric conversions bear some information on the permeability of the formations.

STOCHASTIC JOINT INVERSION

We propose a general algorithm to invert the material properties of the formations (the intrinsic permeability k_0, the porosity ϕ, the electrical conductivity σ, the bulk modulus of the dry porous frame K_{fr}, the bulk modulus of the fluid K_f, the bulk modulus of the solid phase K_s, and the shear modulus of the porous frame G) using a joint inversion of seismic and seismoelectric signals. We use a probabilistic framework to map the distribution of errors in observed data into the model space. In addition, a probabilistic framework can handle easily the nonuniqueness of the inverse problem, which is reflected in the probability distribution of model parameters.

The first criterion for joint inversion requires that the predicted seismic and electroseismic data fit their observed counterparts. Therefore, we perform a Bayesian approach to estimate the material properties $\mathbf{m} = [\mathbf{m}(k_0), \mathbf{m}(\phi), \mathbf{m}(\sigma), \mathbf{m}(K_{fr}), \mathbf{m}(K_s), \mathbf{m}(K_f), \mathbf{m}(G)]$ from seismograms and electrograms where $\mathbf{m}(m_0)$ refers to the logarithm of the different material properties m_0, except for the porosity, which is defined as $\log[\phi/(1-\phi)]$. Indeed, porosity is a concentration of connected voids and is the only material property that is comprised between 0 and 1. This type of transformation is known as the logit transformation. Logit is often used for linearizing sigmoid distributions of proportions (Berkson, 1951). Ghorbani et al. (2007) uses this type of transform to invert induced polarization data in terms of a parameter called the chargeability, which corresponds to a concentration of polarizable elements.

Another point is that we consider the set of material properties (k_0, ϕ, σ, K_{fr}, K_f, K_s, and G) as corresponding to independent properties, and k_0 and $\bar{Q}_V$ as two completely interrelated properties. We also could add additional petrophysical relationships between the porosity on one side and the permeability, electrical conductivity, and bulk modulus of the skeleton on the other side. These relationships could be defined in a probabilistic sense, which would improve the convergence of the inversion. However, we prefer to stay conservative below and to consider these above-mentioned properties as independent.

The Bayesian solution to an inverse problem is based on combining the information coming from geophysical data with some a priori knowledge. In the Bayesian approach, we consider the acquisition of geophysical data as an experiment E. The Bayesian analysis considers the data vector $\mathbf{d}$ and model parameter vector $\mathbf{m}$ of a model M as random variables. Several geometric or petrophysic models M are possible to explain the data. Random variables are characterized with distributions and we assume that all distributions are characterized by probability density functions (Tarantola, 2005).

The objective of inverse modeling is to update the information on $\mathbf{m}$, assuming a petrophysical model or a geometric model M, given the data $\mathbf{d}$ and a priori information regarding $\mathbf{m}$. The a priori information can come from independent observations and petrophysical relationships. In a probabilistic framework, the inverse problem corresponds to maximize the conditional probability of occurring m of M given the data vector $\mathbf{d}$. We note $P_0(\mathbf{m}|\mathrm{M})$ the a priori probability density or belief of parameters $\mathbf{m}$ of model M, and such a model generates the probability density of likelihood $P(\mathbf{d}|\mathbf{m},M)$ corresponding to the data fit.

In a Bayesian approach, the posteriori probability density $\pi(\mathbf{m}|\mathbf{d})$ of the model parameters $\mathbf{m}$ given the data $\mathbf{d}$ is obtained by using Bayes formula

$$\pi(\mathbf{m}|\mathbf{d},M) = \frac{P(\mathbf{d}|\mathbf{m},M)P_0(\mathbf{m}|M)}{P(\mathbf{d}|M)}, \tag{23}$$

where $P(\mathbf{d}|M)$, the evidence, is defined as,

$$P(\mathbf{d}|M) = \int P_0(\mathbf{m}|M)P(\mathbf{d}|\mathbf{m},M)\mathrm{d}\mathbf{m}. \tag{24}$$

This marginal likelihood usually is ignored because it is not a function of the parameters $\mathbf{m}$. For any given model M, the evidence will have a constant value. Consequently, the nature of the evidence is not needed if we are interested only in the nature of the variation of the a posteriori distribution rather than its exact value.

In the following, we assume that the model M is certain. (For example, we know the position of the sedimentary layers and reservoir from seismic data, and we know that the petrophysical model defined by equations 5–10 is exact.) Therefore, we drop the term M from equations 23 and 24. The posteriori probability density $\pi(\mathbf{m}|\mathbf{d})$ of the model parameters $\mathbf{m}$ given the data $\mathbf{d}$ is written as

$$\pi(\mathbf{m}|\mathbf{d}) \propto P(\mathbf{d}|\mathbf{m})P_0(\mathbf{m}). \tag{25}$$

The Bayesian solution of the inverse problem is the whole posterior probability distribution of the material properties. An estimate of unknown parameters can be computed, e.g., as the expectation value with respect to the posterior distribution (i.e., as the mean value) or as the maximum a posteriori value, which can be understood as the most likely value.

As usually accepted, the likelihood function used to assess for the quality of a model $\mathbf{m}$ is Gaussian distributed

$$P(\mathbf{d}|\mathbf{m}) = \frac{1}{[(2\pi)^N \det \boldsymbol{C}_d]^{1/2}} \times \exp\left[-\frac{1}{2}(g(\mathbf{m}) - \mathbf{d})^T \boldsymbol{C}_d^{-1}(g(\mathbf{m}) - \mathbf{d}) \right], \tag{26}$$

$$\mathbf{d} = (\mathbf{d}_S, \mathbf{d}_E)^T, \tag{27}$$

where $g(\mathbf{m})$ is the forward modeling operator for the seismic and seismoelectric semicoupled problem. It nonlinearly connects the generation of seismograms and electrograms to the variation of material properties of the ground, and $\mathbf{d}$ is an N-vector of the observed seismic data $\mathbf{d}_S$ and seismoelectric data $\mathbf{d}_E$. The (NN)-covariance matrix is given by

$$\boldsymbol{C}_d = \begin{bmatrix} \sigma_S^2 & 0 \\ 0 & \sigma_E^2 \end{bmatrix} \tag{28}$$

(where S stands for seismic and E for electrical data). This matrix comprises the measurement errors for the seismic and electrical data, which usually are uncorrelated and assumed to obey Gaussian distributions.

The a priori distribution on the model parameters, if available, also is taken as Gaussian

$$P_0(\mathbf{m}) = \frac{1}{[(2\pi)^M \det \boldsymbol{C}_m]^{1/2}} \times \exp\left[-\frac{1}{2}(\mathbf{m} - \mathbf{m}_{prior})^T \boldsymbol{C}_m^{-1}(\mathbf{m} - \mathbf{m}_{prior}) \right], \tag{29}$$

where $\boldsymbol{m}_{prior}$ is the prior value of distribution of the three petrophysical parameters in the ground, and $\boldsymbol{C}_m$ is the model diagonal covariance matrix incorporating the uncertainties related to the a priori model of material properties. In the example shown in the section entitled "Application to a Synthetic Case Study," we will use a null prior as information on the model parameters.

In the classical Bayesian approach, the model parameters $\mathbf{m}$ that fit the geophysical observations $\mathbf{d}$ maximize the posterior probability density $\pi(\mathbf{m}|\mathbf{d})$. The problem is to explore the posterior probability density $\pi(\mathbf{m}|\mathbf{d})$ expressed by equation 23. The denominator of equation 23 is the normalizing factor required for the integral of the probability density function to be one. Normalizing is not required to perform the inversion, except if we want to compute explicitly the probability for a given parameter to be in a given interval. In addition, the normalization can be done at the end of the computation of the probability density function (restricting to the numerator) just by normalizing it (dividing it by its integral) (Grandis et al., 1999).

The Markov Chain Monte Carlo (MCMC) family of algorithms is well suited for Bayesian inference problems (Mosegaard and Tarantola, 1995; Malinverno and Torres-Verdin, 2000; Malinverno, 2002). MCMC algorithms consist of random walks where different states (i.e., different values of a model vector) are visited, and the choice of the next state depends only on the value of the current state. After an initial period in which the random walker moves toward the highest a posteriori probability regions, the chain returns a number of model vectors sampling the a posteriori probability density $\pi(\mathbf{m}|\mathbf{d})$. The characteristic of the probability density $\pi(\mathbf{m}|\mathbf{d})$, such as the mean and standard deviation or the number of extrema in the probability density, therefore can be determined easily. Memory mechanisms of the MCMC algorithms (that make the chain staying in the high a posteriori probability regions of the model space) are responsible for a greater efficiency of the algorithm in comparison with the Monte Carlo methods for which models are chosen independently and tested against the observations (Sternberg, 1979).

The basic Metropolis-Hastings algorithm is a two-step procedure. In the first step, the current model parameter vector $\mathbf{m}$ in the Markov chain is modified randomly to obtain a candidate vector. This candidate is drawn from a proposal distribution $q(\mathbf{m},\mathbf{m}')$ where the choice of $\mathbf{m}'$ depends on the current vector $\mathbf{m}$. The proposal distribution could be, for example, a multidimensional Gaussian distribution. We denote $q(\mathbf{m},\mathbf{m}')$, the probability density of proposing a model $\mathbf{m}'$, when a model $\mathbf{m}$ and the target density function for sampled model by $\pi(\mathbf{m}|\mathbf{d})$ is the posterior density evaluated at model $\mathbf{m}$. In the second step, the candidate model is accepted with the acceptance probability (Malinverno, 2002),

$$\alpha(\mathbf{m};\mathbf{m}') = \min\left[1, \frac{\pi(\mathbf{m}'|\mathbf{d})}{\pi(\mathbf{m}|\mathbf{d})}\frac{q(\mathbf{m}|\mathbf{m}')}{q(\mathbf{m}'|\mathbf{m})}\right],$$
$$= \min\left[1, \frac{P_0(\mathbf{m}')}{P_0(\mathbf{m})}\frac{P(\mathbf{d}|\mathbf{m}')}{P(\mathbf{d}|\mathbf{m})}\frac{q(\mathbf{m}|\mathbf{m}')}{q(\mathbf{m}'|\mathbf{m})}\right],$$
$$= \min[1, (\text{Prior ratio}).(\text{Likelihood ratio}).(\text{Proposal ratio})]. \quad (30)$$

If the candidate is accepted, the state of the chain is changed to $\mathbf{m}'$, otherwise the chain stays at $\mathbf{m}$. The acceptance probability depends only on the proposal, likelihood, and prior functions at the current and candidate models, all of which can be computed easily. Assuming that the proposal distribution is symmetric, $q(\mathbf{m}'|\mathbf{m}) = q(\mathbf{m}|\mathbf{m}')$ (e.g., a Gaussian distribution centered at the current point), the acceptance probability reduces to:

$$\alpha(\mathbf{m};\mathbf{m}') = \min\left[1, \frac{P(\mathbf{m}'|\mathbf{d})}{P(\mathbf{m}|\mathbf{d})}\right]. \quad (31)$$

This algorithm is known as the original Metropolis algorithm (Metropolis et al., 1953).

To improve the performance of the standard Metropolis-Hasting algorithm, Haario et al. (2001) introduce an algorithm called the adaptive-Metropolis algorithm (AMA) to find the optimal proposal distribution. This algorithm is based on the traditional Metropolis algorithm with a symmetric Gaussian proposal distribution centered at the current model $\mathbf{m}^i$ and with the covariance $\boldsymbol{C}^i$ that changes during the sampling in such a way that the sampling efficiency increases over time (Haario et al., 2001, 2004). The AMA algorithm, though not Markovian, simulates correctly the posterior probability distributions of the model parameters. An important advantage of the AMA algorithm is that it starts using the cumulating information right at the beginning of the simulation. The rapid start of the adaptation ensures that the search becomes more effective at an early stage of the simulation, which diminishes the number of iterations to reach the convergence of the chain.

Table 1. Material properties for the numerical benchmark test.

Parameter	Meaning	Value
σ	Conductivity of the medium	0.01 S m^{-1}
$\bar{Q}_V$	Excess of charge per unit pore volume	1 C m^{-3}
ρ_s	Bulk density of the solid phase	2650 kg m^{-3}
ρ_f	Bulk density of the fluid phase	1000 kg m^{-3}
ϕ	Porosity	0.30
K_s	Bulk modulus of the solid phase	35×10^9 Pa
K_f	Bulk modulus of the fluid phase	2.25×10^9 Pa
G_{fr}	Shear modulus of the frame	11×10^9 Pa
K_{fr}	Bulk modulus of the frame	5×10^9 Pa
k_0	DC permeability	10^{-11} m^2
η_f	Dynamic viscosity of the pore fluid	10^{-3} Pa s

The AMA algorithm is described as follows. Let us assume that we have sampled the states $(\mathbf{m}^0,\ldots,\mathbf{m}^{i-1})$ where $\mathbf{m}^0$ corresponds to the model vector of the initial state. Then a candidate point $\mathbf{m}'$ is sampled from the Gaussian proposal distribution q with mean point at the present point $\mathbf{m}^{i-1}$ and with the covariance

$$\boldsymbol{C}^i = \begin{cases} \boldsymbol{C}^0, & \text{if } i \le n_0, \\ s_n\boldsymbol{K}^i + s_n\varepsilon\boldsymbol{I}_n, & \text{if } i > n_0, \end{cases} \quad (32)$$

where $\mathbf{I}_n$ denotes the n-dimensional identity matrix, $\mathbf{K}^i = \mathrm{Cov}(\mathbf{m}^0,\ldots,\mathbf{m}^{i-1})$ is the regularization factor (a small positive number that prevents the covariance matrix from becoming singular), $\mathbf{C}^0$ is the initial covariance matrix that is strictly positive (note that the AMA algorithm is not too sensitive to the actual values of $\mathbf{C}^0$), and $s_n = (2.4)^2/n$ is a parameter that depends only on the dimension of the vector $\boldsymbol{m} \in \Re^n$ (Haario et al., 2001). According to Gelman et al. (1996), this choice of s_n yields an optimal acceptance in the case of a Gaussian target's distribution and a Gaussian proposal distribution. The candidate model vector $\mathbf{m}'$ is accepted with the acceptance probability:

$$\alpha(\mathbf{m}^{i-1};\mathbf{m}') = \min\left[1, \frac{\pi(\mathbf{m}'|\mathbf{d})}{\pi(\mathbf{m}^{i-1}|\mathbf{d})}\right]. \quad (33)$$

If the candidate model vector is accepted, we consider that $\mathbf{m}^i = \mathbf{m}'$, otherwise we choose $\mathbf{m}^i = \mathbf{m}^{i-1}$.

The AMA algorithm was written in a MATLAB routine that is coupled with the forward modeling made in Comsol Multiphysics 3.5. This algorithm is applied in the next section to the synthetic seismograms and electrograms data to invert the material properties assuming that the position of the geologic units is known.

APPLICATION TO A SYNTHETIC CASE STUDY

Benchmark of the code

The perfectly matched layer (PML) boundary conditions used for the seismic problem are described in detail in Appendix B. We first propose a benchmark test of the reliability of the finite-element code. We simulate the fast and slow P-waves associated with an explosive source in a homogeneous porous material filled with a Newtonian fluid. The dimensions of the 2D domain are 800×800 m^2. The reference of the Cartesian coordinate system O(0, 0) is at the bottom left corner. The time dependence of the source $F(t)$ is a Ricker wavelet with a dominant frequency of 10 Hz. It is located at the source point S(x,y) = (400 m, 400 m). The position of the receiver (observation point) is P(x,y) = (200 m, 300 m). The four edges are absorbing boundaries for which we use PML boundary conditions. The material properties used for this simulation are reported in Table 1. Figure 1 shows the two components (horizontal and vertical) of the displacement of the solid skeleton and the two components of the relative displacement $\mathbf{w}$. The results are shown at 15 Hz. Figure 2 shows the resulting electrical potential distribution. To benchmark the numerical code, we compare the numerical solution with the analytical solution given by Dai et al. (1995). As shown in Figure 2, both solutions are in excellent agreement.

Numerical simulation

To check the usefulness of a joint inversion of seismic and seismoelectric data, we test this approach using a numerical case study. We consider two flat layers plus a rectangular reservoir embedded in the second layer (Figure 3). The geophones and electrodes are located at the top surface of the system to simulate an onshore acquisition. The takeout for the electrodes and geophones is 10 m. The source wavelet is a first-order derivative of a Gaussian as defined in equation 20, with dominant frequency $f_0 = 30$ Hz and with a time delay factor $t_0 = 0.1$ s, see equation 20. The seismic source is located at a depth of 20 m (Figure 3). The true values of the material properties used for the simulation are reported in Table 2. With these values, the velocity of the P-fast wave is 1972 m s^{-1} in the first layer (labeled L1), 2188 m s^{-1} in the second layer (labeled L2), and 3118 m s^{-1} in the reservoir (labeled R). The receiver located with an offset of $x = 150$ m from the source, the time required for the P-wave to reach this receiver is therefore 0.076 s in agreement with the numerical simulations (see below). The finite-element modeling based on Comsol Multiphysics 3.5 is used to simulate seismograms and electrograms at the ground surface.

In Figure 4d, the electrograms show the two types of seismoelectric signals described in the introduction. The first type of signals corresponds to the coseismic electrical signal associated with the propagation of the P-wave. The coseismic electric field related to the direct field wave from the source to the receiver is labeled CS. Other coseismic signals are associated with the reflected P-waves at the various interfaces such as the L1-L2 interface, L2-reservoir interface, and reservoir-L2 interface. These coseismic signals are labeled RCS1, RCS2, and RCS3, respectively. A coseismic signal occurs when a seismic wave travels through a porous material creating a relative displacement between the pore water and the solid phase. The associated current density is balanced by a conduction current density. It results in an electrical field traveling at the same speed as the seismic wave. Because shear waves are equivoluminal, they are not responsible for any source current density in a homogenous medium and therefore they have no coseismic electric field associated with them (Haines and Pride, 2006).

The second type of seismoelectric signals correspond to converted seismoelectric signals associated with the arrival of the P-waves at each interface (between the two layers and at the surface of the reservoir). These converted seismoelectric signals are labeled IR1, IR2, IR3, IR4, and IR5 (see Figures 3–5). When crossing an interface between two domains characterized by different properties, a seismic wave generates a time-varying charge separation, which acts as a dipole radiating electromagnetic energy. In our approach, we neglect the time used by this electromagnetic energy to diffuse from the geologic interface, where it is generated, to the receiver (quasi-static field approximation). This assumption is very good for investigations to the first kilometers below the ground surface. Because of constructive interferences, a significant portion of the first Fresnel zone acts as a disk of electric dipoles oriented normal to the interface. These dipoles oscillate with the waveform of the seismic wave (Figure 4b). Because the electromagnetic diffusion of the electrical disturbance is very fast, the seismoelectric conversions are observed nearly at the same time by all the electrodes, but with different amplitudes. The seismoelectric conversions appear therefore as flat lines in the electrograms. Also note that the polarity of the converted seismoelectric signals depends on the contrast of electrical material properties (volumetric charge density and electrical conductivity) at the interface where they are generated. On the contrary, the polarity of the coseismic electrical signals depends on the value of the streaming potential coupling coefficient at the position of the electrode and the polarity of the seismic waves.

Figure 5 shows the electric potential for a given electrode. In this figure, we clearly can discriminate the coseismic signals from seismoelectric conversions. Also note that amplitudes of the signals are small. However, they can be measured easily in the field using the type of ultrasensitive equipment discussed by Crespy et al. (2008).

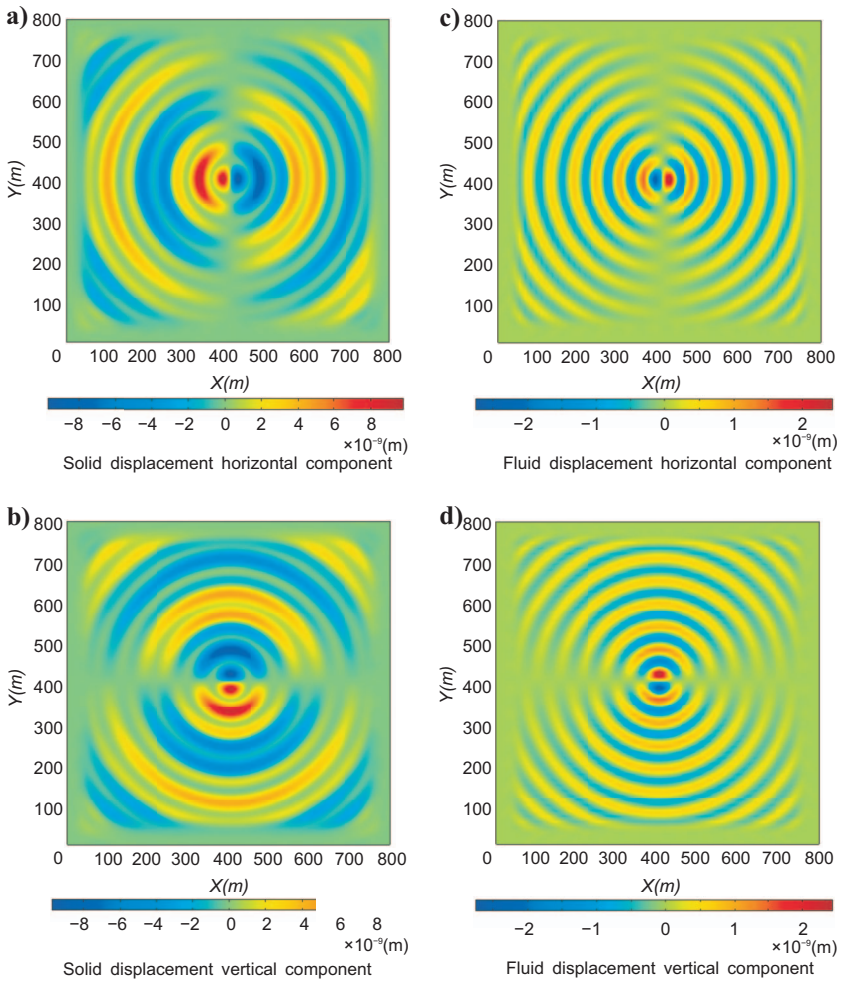

Figure 1. Horizontal and vertical components of the solid displacement vector and relative fluid displacement in the frequency domain (real components). Note the efficiency of the C-PML approach at the boundaries to attenuate the seismic waves.

This equipment can be used to record electrical potential using up to 256 simultaneous channels at several kHz and with a sensitivity of 10 nV.

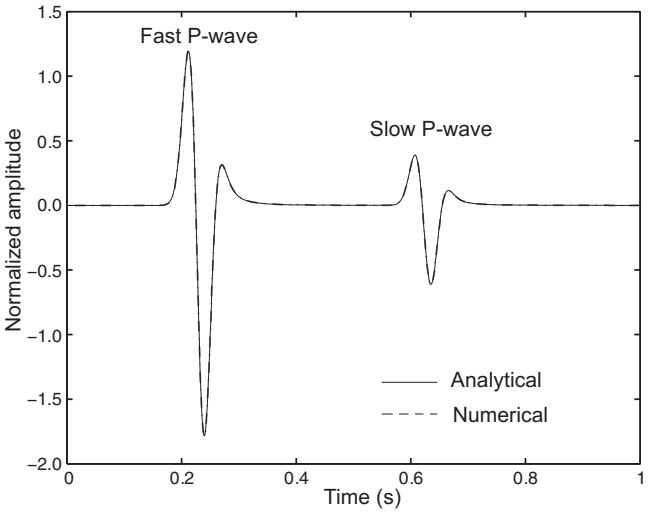

Figure 2. Comparison between analytic and numerical solution of the seismic problem in an homogeneous medium (benchmark test) with properties summarized in Table 1. The figure shows a snapshot of the vertical-component of the macroscopic solid displacement at $t = 0.58$ s. The two P-waves can be observed. The synthetic numerical seismograms (solid black line) and analytical solution calculated by Dai et al. (1995) are in very close agreement.

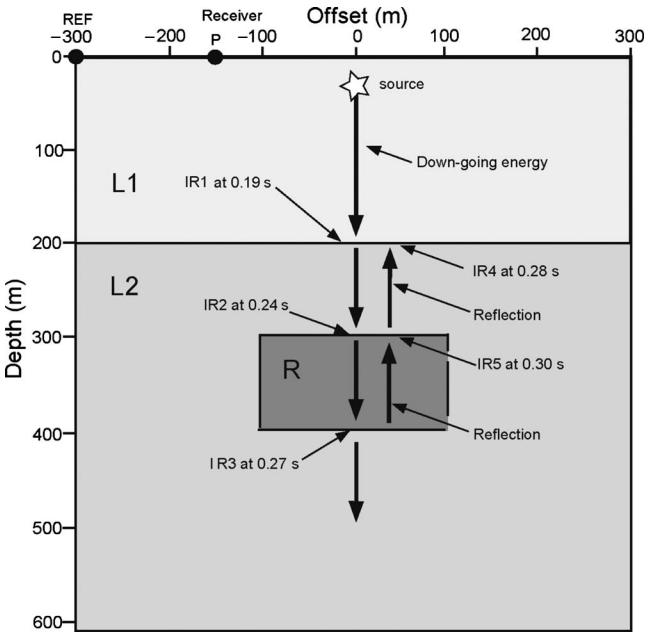

Figure 3. Sketch of the model used for the simulations. The geophones and electrodes are collocated at the top surface of the system. All the electrodes are assumed to be connected to a reference electrode. The REF corresponds to the position of the reference electrode. Labels L1 and L2 correspond to the two layers of sediments and R stands for the reservoir. Arrows indicate raypath for seismic energy that creates seismoelectric interface response labeled IRi. In addition to this energy, the direct field and reflected seismic arrivals are recorded as coseismic electric field. The seismic source is located at a depth of 20 m below the top surface.

Result of the joint inversion

We use the AMA algorithm described in the section entitled "Stochastic Joint Inversion" to generate 25,000 realizations of the 21 parameters of the material properties of the different geologic units, using the data recorded in 60 geophones and 60 electrodes at only four frequencies (25, 30, 35, and 40 Hz). The position and characteristic of the source are assumed to be perfectly known. The posterior probability distribution functions of the material properties of the three units (layers L1 and L2 and the reservoir R) are shown in Figure 6 using the last 5000 iterations. We observe that, except for the porosity, our algorithm is performing a very good job in inverting properly the seismic and seismoelectric data in terms of getting the mean value of the material properties. We believe that a better estimate of the porosity can be obtained through the use of additional petrophysical relationships between the porosity, electrical conductivity, and bulk modulus of the skeleton.

DISCUSSION

In this section, we want to answer the following questions: Is the sensitivity of existing tools high enough to record the seismoelectric conversions? Is the present approach directly useable to invert real data? And if not, what needs to be added?

Crespy et al. (2008) show that electroencephalographic equipment can be used to provide reliable electrograms with a sensitivity better than 0.1 μV up to a frequency of few kHz. In marine CSEM, the measurement of the electrical field is often made with sensitivity on the order of 1 nV once the spurious electromagnetic effect of external origin has been filtered out. A new generation of electrodes exist, developed for EM studies, that couple with the ground or seafloor by capacitance rather than resistance. These electrodes show usually five times lower noise than nonpolarizing Ag/AgCl in the frequency range 1–10 Hz. So we believe that, although difficult, accurate measurements of seismoelectric conversions produced at a depth of a few hundred meters below the sensors, or for cross-hole investigations, is possible. Consequently, seismoelectric investigations made onshore could benefit from all the recent developments made in

Table 2. True values of the material properties used for the synthetic model shown in Figure 3. L1 and L2 stand for the two layers and R for the reservoir (see Figure 3). Layer L1 corresponds to a clean sand, L2 to a clayey sand, and R to a sand reservoir partially filled with oil.

Parameter	Units	Unit L1	Unit L2	Unit R
k_0	m^2	10^{-12}	10^{-16}	10^{-11}
ϕ	GPa	0.25	0.10	0.33
K_s	GPa	36.50	6.90	37.00
K_f	GPa	0.25	0.25	2.40
K_{fr}	GPa	2.22	6.89	9.60
G	kg m^{-3}	4.00	3.57	5.00
ρ_s	kg m^{-3}	2650	2650	2650
ρ_f	Pa s	1040	1040	983
η_f	S m^{-3}	1×10^{-3}	1×10^{-3}	8×10^{-1}
σ	Log C m^{-3}	0.01	0.1	0.001
Log $\bar{Q}_V$		0.203	3.49	3.2

measuring small electrical fields at the seafloor for controlled source EM methods (CSEM) (see Ellingsrud et al., 2008).

The second point concerns the direct application of the present approach to real data. Because our approach is based on full waveform modeling of the seismoelectric and seismic wavefields, it requires seriously taking into account the problem of wave attenuation except at low frequencies (few Hertz) for which attenuation can be neglected. Our approach needs just to be modified slightly to account for real attenuation mechanisms that are not described by the classical Biot theory. The trick usually is to replace a perfect poroelastic behavior by a viscoelastic behavior to match the attenuation of the various mechanical waves (see Morency and Tromp [2008] for a complete development). With such a modified theory, we can apply our approach to real data and add the intrinsic attenuation mechanisms in the inversion algorithm as additional unknown parameters.

One should note that surface waves have been discarded in the modeling proposed in the sections above. In reality, these impose a real constraint on the measurement system in terms of dynamic range because they are orders of magnitude larger than the interfacial signals. However, as for the electromagnetic disturbance related to the source itself, the electromagnetic disturbance associated with the passage of the surface wave can be filtered out of the signals. The idea is to ignore the data recorded at the time of the passage of the surface wave from the record. Also note that for onshore records, the intensity of the electrical field associated with the passage of the surface waves depends on the value of the streaming potential coupling coefficient at the position of the recording dipoles. Because the coupling coefficient decreases linearly with the effective saturation, this depends in turn on the water content near the dipoles of electrodes. Water content below the residual water saturation would not create an electrical field. Finally, we want to draw the attention of the readers to the large amount of technologies that have been developed in medical sciences (the use of capacitive electrodes for instance to measure the electrocardiogram of a human heart without electric

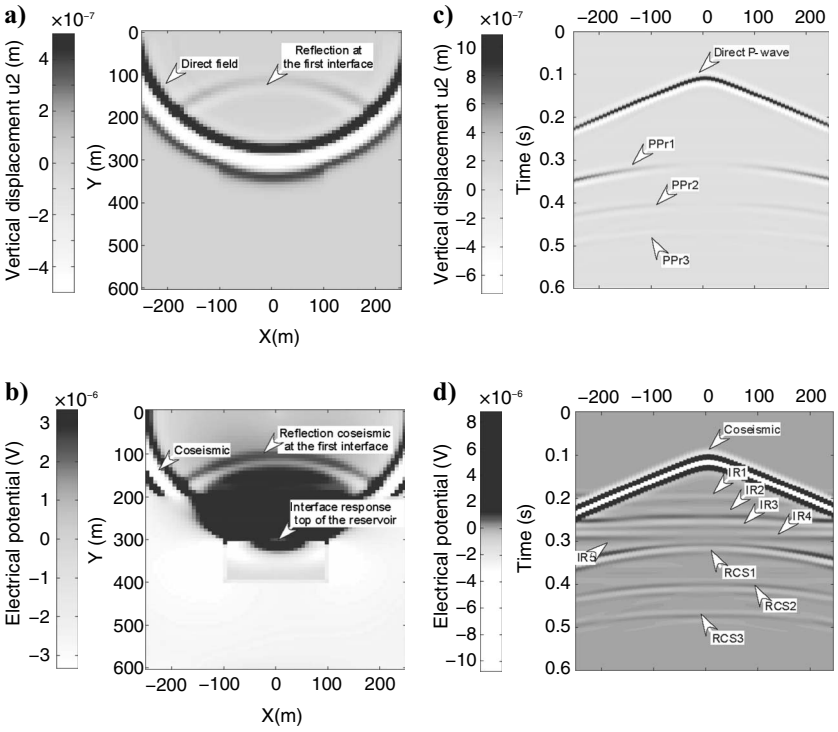

Figure 4. Snapshots of seismic and seismoelectric phenomena. (a and b) Snapshots of the seismic and electrical fields at time $t = 0.24$ s. This corresponds to the time when the P-wave reaches the top of the reservoir, which acts as a dipole radiating electromagnetic energy. (c) The seismograms reconstructed by the geophones (with a take out of 10 m) present direct field and different reflection of the P-waves: the reflection PPr1 on the interface L1-L2, the reflection PPr2, on the interface L2-top of the reservoir, and the reflection PPr3 on the interface L2-bottom of the reservoir. (d) The electrograms show the coseismic electrical potential field associated with the direct wave and with the reflections of the P-wave (labeled RCS1, RCS 2, RCS 3) and the seismoelectric conversions with a smaller amplitude and a flat shape (labeled IR1, IR2, IR3, IR4, IR5).

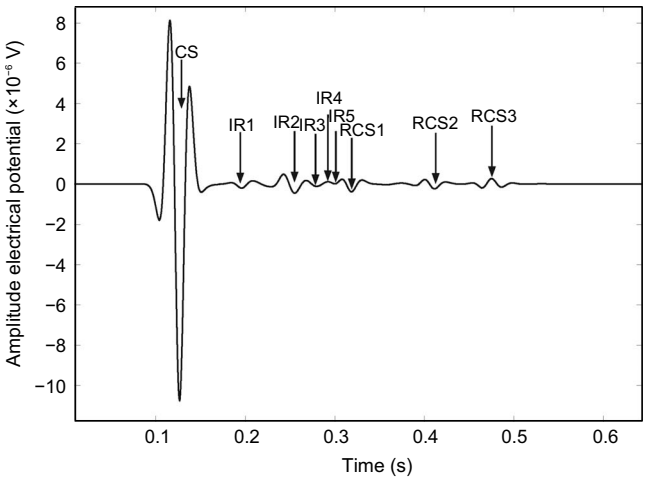

Figure 5. Electrogram at an electrode (receiver) with a horizontal offset of 150 m. The CS stands for the coseismic disturbance associated with the direct wave (see Figure 1). The RCS1 and RCS2 stand for the coseismic disturbances associated with the reflected P-waves (see Figure 1). IRi stand for the various seismoelectric disturbances associated with the seismoelectric conversions at the different interfaces of the system.

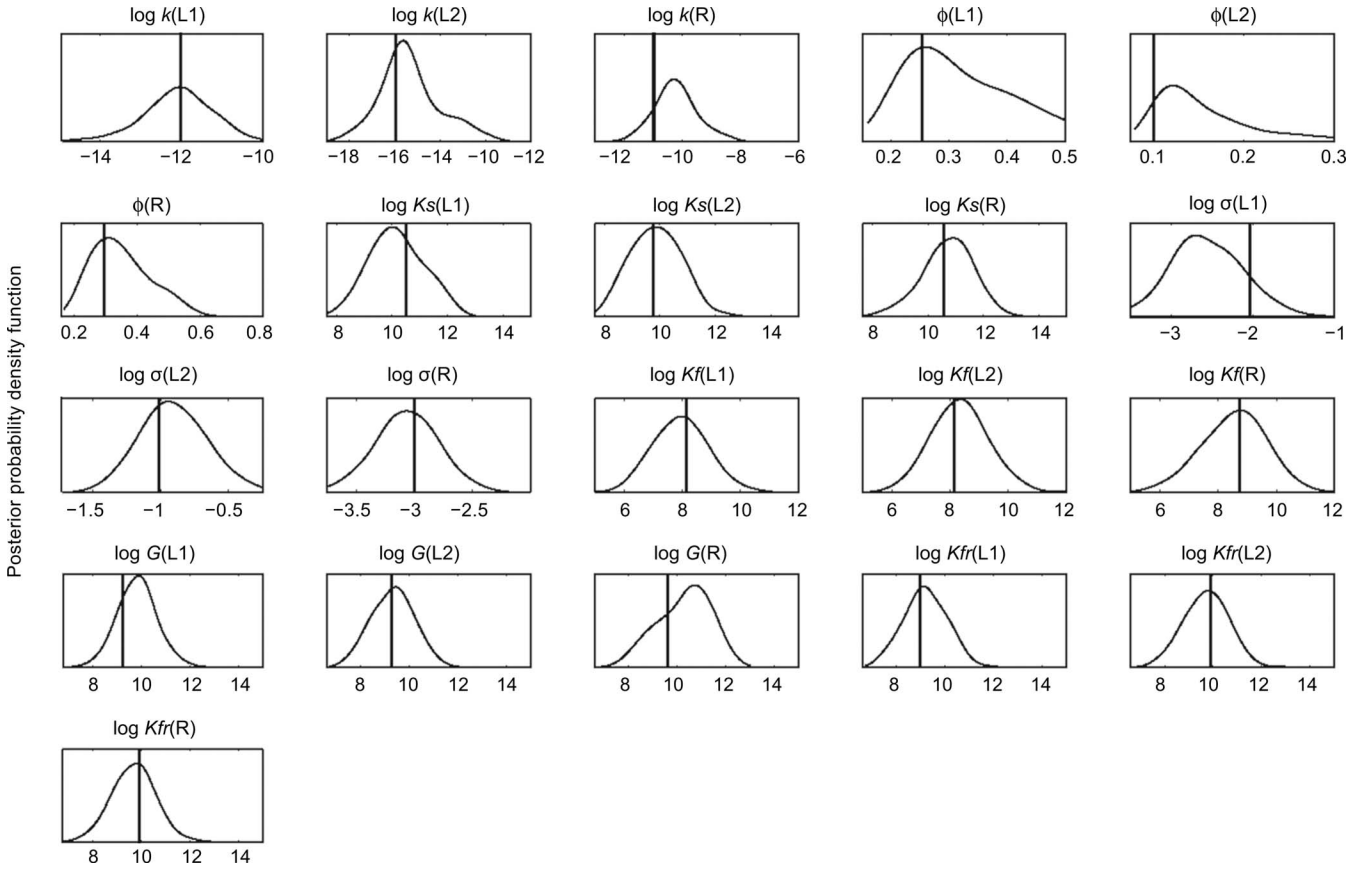

Figure 6. Posterior probability density functions of the material properties for the three geological units (the two layers L1 and L2 and the reservoir R). The vertical bars indicate the real value of the material properties (see Table 1).

contact with the skin, see Oehlerm et al. [2008] or in electroencephalography, see Okazaki and Nakazoe [2005]), which have not yet been applied to seismoelectric signals despite many common characteristics for these problems.

CONCLUSIONS

We have developed a stochastic algorithm to perform the joint inversion of seismic and seismoelectric data in heterogeneous systems to retrieve the value of the material properties of individual units (e.g., sedimentary layers, faults, or geologic reservoirs). The model is based on the classical equations of poroelasticity and an electrokinetic formulation that was developed initially to model the quasi-static self-potential response associated with the flow of groundwater. We have reached the following conclusions: A stochastic inversion algorithm can be used to invert jointly seismic and seismoelectric data; the permeability of the formation can be recovered within one order of magnitude; porosity is not well constrained by the inversion; we also can invert the electrical conductivity of the formations and poroelastic mechanical formation properties. The ability to invert for electrical conductivity is good news because electrical conductivity usually depends strongly on the oil saturation in the reservoir. Therefore, this can be a way to determine the in situ oil saturation.

The next step will be also to include in the inversion of the electrograms and seismograms, the position of the boundaries between the different formations and to extend the code to multiphase conditions in 3D.

ACKNOWLEDGMENTS

We thank Terry Young for his support at CSM. We thank T. Müller, N. Florsch, and two anonymous referees for their very constructive reviews.

APPENDIX A

THE FIELD EQUATIONS

We start with the Darcy equation with the electro-osmotic coupling term neglected,

$$\frac{\eta_f}{k(\omega)}\dot{\mathbf{w}} = -\nabla p - \rho_f \ddot{\mathbf{u}} + F_f, \qquad \text{(A-1)}$$

where $\mathbf{F}_f$ is the body force acting on the pore fluid phase. The fact that the electro-osmotic term can be neglected safely has been discussed by a number of authors (see, for instance, Revil et al., 1999). The dynamic permeability is written as (e.g., Morency and Tromp, 2008)

$$\frac{1}{k(\omega)} \equiv \frac{1 - j(\omega/\omega_c)}{k_0}, \tag{A-2}$$

which follows from the low-frequency approximation to the dynamic permeability given by Pride (1994). The critical frequency is $\omega_c = \eta_f/(k_0\rho_f F) = b/\tilde{\rho}_f$ where $b = \eta_f/k_0$ and $\tilde{\rho}_f = \rho_f F$. Neglecting the body force acting on the fluid phase, equation A-1 can be used to express the filtration displacement $\mathbf{w}$ as a function of the pore fluid pressure p and the displacement of the solid phase $\mathbf{u}$,

$$\mathbf{w} = k_\omega(\nabla p - \omega^2\rho_f\mathbf{u}), \tag{A-3}$$

where k_ω is defined by

$$k_\omega = \frac{1}{\omega^2\tilde{\rho}_f + j\omega b}. \tag{A-4}$$

Equation A-3 can be used in Newton's law to give

$$-\omega^2\rho_\omega^s\mathbf{u} - \omega^2\rho_f k_\omega\nabla p = \nabla\cdot\mathbf{T}, \tag{A-5}$$

$$\rho_\omega^s = \rho - \omega^2\rho_f^2 k_\omega, \tag{A-6}$$

where ρ_ω^s is an apparent mass density for the solid phase. Equation A-5 is a partial differential equation between $\mathbf{u}$ and p, but the stress tensor $\mathbf{T}$ also depends on $\mathbf{w}$. Using the relationships between the stress and strain, we obtain the following relationship between the divergence of the filtration displacement $\nabla\cdot\mathbf{w}$ and the divergence of the displacement of the solid phase $\nabla\cdot\mathbf{u}$,

$$\nabla\cdot\mathbf{w} = -\frac{1}{M}(p + S) - \alpha\nabla\cdot\mathbf{u}, \tag{A-7}$$

where α is the classical Biot coefficient of poroelasticity, defined by equations 7 and 10. We use this equation A-7 in the stress/strain relationships to remove the dependence of the stress tensor $\mathbf{w}$. This yields

$$\mathbf{T} = \lambda(\nabla\cdot\mathbf{u})\mathbf{I} + G[\nabla\mathbf{u} + \nabla\mathbf{u}^{\mathrm{T}}] - \alpha p\mathbf{I}, \tag{A-8}$$

$$\lambda = K - \frac{2}{3}G, \tag{A-9}$$

where λ is the Lamé modulus of the skeleton. The effective stress tensor is written as

$$\hat{\mathbf{T}} = \lambda(\nabla\cdot\mathbf{u})\mathbf{I} + G[\nabla\mathbf{u} + \nabla\mathbf{u}^{\mathbf{T}}], \tag{A-10}$$

$$\mathbf{T} = \hat{\mathbf{T}} - \alpha p\mathbf{I}. \tag{A-11}$$

The effective stress tensor is the equivalent stress tensor of the skeleton without fluid (in vacuo). Using equations A-6–A-9 and A-3, we obtain an equation connecting the solid displacement and the fluid pressure assuming that the Biot coefficient is constant,

$$-\omega^2\rho_\omega^s\mathbf{u} + \theta_\omega\nabla p = \nabla\cdot\hat{\mathbf{T}}, \tag{A-12}$$

$$\theta_\omega = \alpha - \rho_f\omega^2 k_\omega, \tag{A-13}$$

where θ_ω is a volumetric hydromechanical coupling coefficient. Equation A-12 corresponds to Newton's law for a poroelastic body. This equation is similar to the classical Newton's law for an elastic solid except the coupling term $\theta_w\nabla_p$, which accounts for the dynamic coupling between the pore fluid and solid phase.

Regarding the description of the filtration displacement, the use of equations 11 and 12 yields the following relationship between $\mathbf{w}$, $\mathbf{u}$, and p:

$$\frac{1}{M}(p + S) + \nabla\cdot\{k_\omega[\nabla p - \omega^2\rho_f\mathbf{u}]\} = -\alpha\nabla\cdot\mathbf{u}. \tag{A-14}$$

Equation A-12 is the diffusion equation for the pore fluid pressure with a source term related to the harmonic change of displacement of the solid phase.

APPENDIX B

PERFECTLY MATCHED LAYER BOUNDARY CONDITIONS

Equations 11, 12, and 14 describe the propagation of seismic waves in an infinite unbounded medium. However, when one performs numerical simulations, the domain investigated is always bounded. A common approach to limit reflection at the boundaries of the domain is to use the one-way wave equation based on the paraxial approximations of the seismic wave equations (Clayton and Engquist, 1977). The perfectly matched layer (PML) method has been proposed later by Berenger (1994), first for electromagnetic problems. Then it has been applied successfully to various wave propagation problems (Chew and Weedon, 1994; Zeng and Liu, 2001; Zeng et al., 2001). With PML boundary layers, almost no reflection is expected to occur at the interface between the physical domain and absorbing layer for any frequency and any angle of incidence of the seismic waves.

In this study, we use the convolution-perfectly matched layer (C-PML) approach. The C-PML method, for the first-order system of partial differential equations, has been developed for electromagnetic waves by Roden and Gedney (2000) and in simulation of elastic waves propagation by Bou Matar et al. (2005). It has never been used for the problem of poroelastic waves, and we adapted this method for this type of problem. This method is extended for second-order systems written in terms of displacements. The main advantages of the C-PML approach over the classical PML approach concerns its numerical stability and its high efficiency. Using the concept of complex coordinates (Chew and Weedon, 1994) in the frequency domain (with a time dependence of $e^{-j\omega t}$), the complex coordinate stretching variables are

$$\tilde{x}_i = \int_0^{x_i} s_{x_i}(x')dx', \quad i = 1,2, \tag{B-1}$$

$$s_{x_i} = k_{x_i}(x_i) + \frac{\sigma_{x_i}(x_i)}{\alpha_{x_i} + j\omega}, \tag{B-2}$$

where α_{x_i}, σ_{x_i} are positive real damping coefficients and k_{x_i} are real and positive-definite numbers that are equal or larger than unity. In this paper, we consider $k_{x_i} = 1$ to keep the waves continuous (for details see Collino and Tsogka, 2001). To determine the value of the two other damping coefficients, we use the following formula:

$$\sigma_i = \begin{cases} \dfrac{3c}{2L_0}\log\left(\dfrac{1}{R}\right)\left(\dfrac{x_{i\,min}-x_i}{L_0}\right)^3, & \text{as } x_{i\,min} \geq x_i, \\ 0, & \text{as } x_{i\,min} \leq x_i \leq x_{i\,max}, \\ \dfrac{3c}{2L_0}\log\left(\dfrac{1}{R}\right)\left(\dfrac{x_i-x_{i\,max}}{L_0}\right)^3, & \text{as } x_i \geq x_{imax}, \end{cases} \tag{B-3}$$

$$\alpha_i = \begin{cases} \pi f_0\left(\dfrac{x_{i\,min}-x_i}{L_0}+1\right), & \text{as } x_{i\,min} \geq x_i, \\ \pi f_0, & \text{as } x_{i\,min} \leq x_i \leq x_{i\,max}, \\ \pi f_0\left(\dfrac{x_i-x_{i\,max}}{L_0}+1\right), & \text{as } x_i \geq x_{i\,max}, \end{cases} \tag{B-4}$$

where c is the highest velocity in the domain, $R = 1/1000$ represents the amount of reflected energy at the outer boundary of the PML layer, L_0 is the thickness of the PML, and f_0 is the dominant frequency of the source.

The derivative $\partial(\cdot)/\partial\tilde{x}_i$ can be expressed in terms of the regular coordinate stretching variables $\partial(\cdot)/\partial\tilde{x}_i = (1/S_{x_i})(\partial(\cdot)/\partial x_i)$. Finally, after replacing $\partial(\cdot)/\partial x_i$ by $\partial(\cdot)/\partial\tilde{x}_i$ and after some algebraic manipulations, the reduced set of equations for the modified poroelastic formulation is:

$$-w^2\tilde{\rho}_w^s\mathbf{u} + \tilde{\boldsymbol{\theta}}_w\nabla p = \nabla\cdot\tilde{\mathbf{T}}, \tag{B-5}$$

$$\tilde{\boldsymbol{\theta}}_w = \begin{pmatrix} \theta_w s_{x_2} & 0 \\ 0 & \theta_w s_{x_1} \end{pmatrix}, \tag{B-6}$$

$$\tilde{\rho}_w^s = \rho_w^s s_{x_1} s_{x_2}, \tag{B-7}$$

$$\tilde{\mathbf{T}} = \begin{pmatrix} \tilde{T}_{11} & \tilde{T}_{12} \\ \tilde{T}_{21} & \tilde{T}_{22} \end{pmatrix}, \tag{B-8}$$

$$\tilde{T}_{11} = (\lambda+2G)\frac{s_{x_2}}{s_{x_1}}\frac{\partial u_1}{\partial x_1} + \lambda\frac{\partial u_2}{\partial x_2}, \tag{B-9}$$

$$\tilde{T}_{22} = \lambda\frac{\partial u_1}{\partial x_1} + (\lambda+2G)\frac{s_{x_1}}{s_{x_2}}\frac{\partial u_2}{\partial x_2}, \tag{B-10}$$

$$\tilde{T}_{12} = G\left(\frac{s_{x_1}}{s_{x_2}}\frac{\partial u_1}{\partial x_2} + \frac{\partial u_2}{\partial x_1}\right), \tag{B-11}$$

$$\tilde{T}_{21} = G\left(\frac{\partial u_1}{\partial x_2} + \frac{s_{x_2}}{s_{x_1}}\frac{\partial u_2}{\partial x_1}\right), \tag{B-12}$$

$$\frac{s_{x_1}s_{x_2}}{M}p + \nabla\cdot[\,\tilde{\mathbf{k}}_{1\omega}\nabla p - \tilde{\mathbf{k}}_{2\omega}\omega^2\rho_f\mathbf{u})] = -\alpha s_{x_1}s_{x_2}\nabla\cdot\mathbf{u}, \tag{B-13}$$

$$\tilde{\mathbf{k}}_{1\omega} = \begin{pmatrix} k_\omega s_{x_2}/s_{x_1} & 0 \\ 0 & k_\omega s_{x_1}/s_{x_2} \end{pmatrix}, \quad \text{and} \tag{B-14}$$

$$\tilde{\mathbf{k}}_{2\omega} = \begin{pmatrix} k_\omega s_{x_2} & 0 \\ 0 & k_\omega s_{x_1} \end{pmatrix}. \tag{B-15}$$

For the electrical problem, we solve the following modified equations:

$$\nabla\cdot(\tilde{\sigma}\nabla\psi) = \nabla\cdot\tilde{\mathbf{j}}_S, \tag{B-16}$$

$$\tilde{\mathbf{j}}_S = (j_{x_1}s_{x_2}; j_{x_1}s_{x_1}), \quad \text{and} \tag{B-17}$$

$$\tilde{\sigma} = \begin{pmatrix} \sigma\dfrac{s_{x_2}}{s_{x_1}} & 0 \\ 0 & \sigma\dfrac{s_{x_1}}{s_{x_2}} \end{pmatrix}. \tag{B-18}$$

REFERENCES

Atalla, N., R. Panneton, and P. Debergue, 1998, A mixed displacement-pressure formulation for poroelastic materials: Journal of the Acoustical Society of America, **104**, 1444–1452.

Berenger, J. P., 1994, A perfectly matched layer for the absorption of electromagnetic waves: Journal of Computational Physics, **114**, 185–200.

Berkson, J., 1951, Why I prefer logits to probits: Biometrics, **7**, 327–339.

Biot, M. A., 1956a, Theory of propagation of elastic waves in a fluid-saturated porous solid, I. Low-frequency range: Journal of the Acoustical Society of America, **28**, 168–178.

———, 1956b, Theory of propagation of elastic waves in a fluid-saturated porous solid, II. Higher-frequency range: Journal of the Acoustical Society of America, **28**, 178–191.

Biot, M. A., and D. G. Willis, 1957, The elastic coefficients of the theory of consolidation: Journal of Applied Mechanics, **24**, 594–601.

Block, G. I., and J. G. Harris, 2006, Conductivity dependence of seismoelectric wave phenomena in fluid-saturated sediments: Journal of Geophysical Research, **111**, B01304, doi: 10.1029/2005JB003798.

Bockris, J. O., and A. K. N. Reddy, 1970, Modern Electrochemistry 2: Plenum Press.

Bolève, A., A. Revil, F. Janod, J. L. Mattiuzzo, and A. Jardani, 2007, Forward modeling and validation of a new formulation to compute self-potential signals associated with ground water flow: Hydrology and Earth System Sciences, **11**, 1661–1671.

Bou Matar, O., V. Prebrazhensky, and P. Pernod, 2005, Two-dimensional axisymmetric numerical simulation of supercritical phase conjugation of ultrasound in active solid media: Journal of the Acoustical Society of America, **118**, 2880–2890.

Butler, K. E., R. D. Russell, A. W. Kepic, and M. Maxwell, 1997, Measurement of the seismoelectric response from a shallow boundary: Geophysics, **61**, 1769–1778.

Chew, W. C., and W. H. Weedon, 1994, A 3-D perfectly matched medium from modified Maxwell's equations with stretched coordinates: Microwave and Optical Technology Letters, **7**, 599–604.

Clayton, R., and B. Engquist, 1977, Absorbing boundary conditions for acoustic and elastic wave equations: Bulletin of the Seismological Society of America, **67**, 1529–1540.

Collino, F., and C. Tsogka, 2001, Application of the PML absorbing layer model to the linear elastodynamic problem in anisotropic heterogeneous media: Geophysics, **66**, 294–307

Crespy, A., A. Revil, N. Linde, S. Byrdina, A. Jardani, A. Bolève, and P. Hen-

ry, 2008, Detection and localization of hydromechanical disturbances in a sandbox using the self-potential method: Journal of Geophysical Research, **113**, B01205, doi: 10.1029/2007JB005042.
Dai, N., A. Vafidias, and E. R. Kanasewich, 1995, Wave propagation in heterogeneous porous media: a velocity-stress, finite-difference method: Geophysics, **60**, 327–340.
Dupuis, J. C., K. E. Butler, and A. W. Kepic, 2007, Seismoelectric imaging of the vadose zone of a sand aquifer: Geophysics, **72**, no. 6, A81–A85.
Ellingsrud, S., T. Eidesmo, and K. M. Strack, 2008, CSEM: a fast growing technology: Presented at the 78th Annual International Meeting, SEG.
Fourie, F. D., 2003, Application of electroseismic techniques to geohydrological investigations in Karoo Rocks: Ph.D. Thesis, University of the Free State.
Frenkel, J., 1944, On the theory of seismic and seismoelectric phenomena in a moist soil: Journal of Physics (USSR), **8**, no. 4, 230–241.
Garambois, S., and M. Dietrich, 2002, Full waveform numerical simulations of seismoelectromagnetic wave conversions in fluid-saturated stratifed porous media: Journal of Geophysical Research, **107**, no. B7, 2148, doi: 10.1029/2001JB000316.
Geertsma, J., and D. C. Smit, 1961, Some aspects of elastic wave propagation in fluid-saturated porous solids: Geophysics, **26**, 169–181.
Gelman, A. G., G. O. Roberts, and W. R. Gilks, 1996, Efficient Metropolis jumping rules, in J. M. Bernardo, J. O. Berger, A. P. Dawid, and A. F. M. Smith, eds., Bayesian statistics 5: Oxford Univ. Press, Inc., 599–608.
Ghorbani, A., C. Camerlynck, N. Florsch, P. Cosenza, A. Tabbagh, and A. Revil, 2007, Bayesian inference of the Cole-Cole parameters from time and frequency-domain induced polarization: Geophysical Prospecting, **55**, 589–605, doi: 10.1111/j.1365-2478.2007.00627.x.
Grandis, H., M. Menvielle, and M. Roussignol, 1999, Bayesian inversion with Markov chains, I. The magnetotelluric one-dimensional case: Geophysical Journal International, **138**, 757–768.
Haario, H., M. Laine, M. Lehtinen, E. Saksman, and J. Tamminen, 2004, MCMC methods for high dimensional inversion in remote sensing: Journal of the Royal Statistical Society, Series B, **66**, 591–607.
Haario, H., E. Saksman, and J. Tamminen, 2001, An adaptive Metropolis algorithm: Bernoulli, **7**, no. 2, 223–242.
Haartsen, M., W. Dong, and M. N. Toksöz, 1998, Dynamic streaming currents from seismic point sources in homogeneous poroelastic media: Geophysical Journal International, **132**, 256–274.
Haartsen, M. W., and S. R. Pride, 1997, Electroseismic waves from point sources in layered media: Journal of Geophysical Research, **102**, no. B11, 24745–24769.
Haines, S. S., S. L. Klemperer, and B. Biondi, 2007, Seismoelectric imaging of shallow targets: Geophysics, **72**, no. 2, G9–G20.
Haines, S., and S. Pride, 2006, Seismoelectric numerical modeling on a grid: Geophysics, **71**, no. 6, N57–N65.
Jardani, A., A. Revil, A. Bolève, J. P. Dupont, W. Barrash, and B. Malama, 2007, Tomography of groundwater flow from self-potential (SP) data: Geophysical Research Letters, **34**, L24403, doi: 10.1029/2007GL031907.
Karpfinger, F., T. M. Müller, and B. Gurevich, 2009, Green's functions and radiation patterns in poroelastic solids revisited: Geophysical Journal International, **178**, 327–337, doi: 10.1111/j.1365-246X.2009.04116.x.
Kulessa, B., T. Murray, and D. Rippin, 2006, Active seismoelectric exploration of glaciers: Geophysical Research Letters, **33**, L07503, doi: 10.1029/2006GL025758.
Leroy, P., and A. Revil, 2004, A triple layer model of the surface electrochemical properties of clay minerals: Journal of Colloid and Interface Science, **270**, 371–380.
Linde, N., D. Jougnot, A. Revil, S. K. Matthaï, T. Arora, D. Renard, and C. Doussan, 2007, Streaming current generation in two-phase flow conditions: Geophysical Research Letters, **34**, no. 3, L03306, doi: 10.1029/2006GL028878.
Malinverno, A., 2002, Parsimonious Bayesian Markov chain Monte Carlo inversion in a nonlinear geophysical problem: Geophysical Journal International, **151**, 675–688.
Malinverno, A., and C. Torres-Verdin, 2000, Bayesian inversion of DC electrical measurements with uncertainties for reservoir monitoring: Inverse problems, **16**, 1343–1356.
Metropolis, N., A. W. Rosenbluth, M. N. Rosenbluth, A. H. Teller, and E. Teller, 1953, Equations of state calculations by fast computing machine: Journal of Chemical Physics, **21**, 1087–1091.
Migunov, N., and A. Kokorev, 1977, Dynamic properties of the seismoelectric effect of water saturated rocks: Izvestiya, Earth Physics, **13**, 443–446.
Mikhailov, O. V., M. W. Haartsen, and M. N. Toksöz, 1997, Electroseismic investigation of the shallow subsurface: Field measurements and numerical modelling: Geophysics, **62**, 97–105.
Mikhailov, O. V., J. Queen, and M. N. Toksöz, 2000, Using borehole electroseismic measurements to detect and characterize fractured (permeable) zones: Geophysics, **65**, 1098–1112.
Morency, C., and J. Tromp, 2008, Spectral-element simulations of wave propagation in porous media: Geophysical Journal International, **175**, 301–345.
Mosegaard, K., and A. Tarantola, 1995, Monte Carlo sampling of solutions to inverse problems: Journal of Geophysical Research, **100**, no. B7, 12431–12447.
Oehlerm, M., V. Ling, K. Melhorn, and M. Schilling, 2008, A multichannel portable ECG system with capacitive sensors: Physiological Measurement, **29**, 783–793, doi: 10.1088/0967-3334/29/7/007.
Okazaki, Y., and J. Nakazoe, 2005, Modulation-type capacitive electrode driven by small AC current for measuring DC biological signals: Systems and Computers in Japan, **36**, no. 13, 69–80.
Pain, C. C., J. H. Saunders, M. H. Worthington, J. M. Singer, W. Stuart-Bruges, G. Mason, and A. Goddard, 2005, A mixed finite-element method for solving the poroelastic Biot equations with electrokinetic coupling: Geophysical Journal International, **160**, 592–608.
Plona, T. J., 1980, Observation of a second bulk compressional wave in a porous medium at ultrasonic frequencies: Applied Physics Letters, **36**, 259–261.
Pride, S., 1994, Governing equations for the coupled electromagnetics and acoustics of porous media: Physical Review B, **50**, no. 21, 15678–15696.
Pride, S. R., and M. W. Haartsen, 1996, Electroseismic wave properties: Journal of the Acoustical Society of America, **100**, no. 3, 1301–1315.
Ranada Shaw, A., A. I. M. Denneman, and C. P. A. Wapenaar, 2000, Porosity and permeability effects on seismo-electric reflection: Presented at the EAGE/SAID Conference.
Revil, A., 2007, Thermodynamics of transport of ions and water in charged and deformable porous media: Journal of Colloid and Interface Science, **307**, 254–264.
Revil, A., and P. Leroy, 2001, Hydroelectric coupling in a clayey material: Geophysical Research Letters, **28**, no. 8, 1643–1646.
Revil, A., and N. Linde, 2006, Chemico-electromechanical coupling in microporous media: Journal of Colloid and Interface Science, **302**, 682–694.
Revil, A., N. Linde, A. Cerepi, D. Jougnot, S. Matthäi, and S. Finsterle, 2007, Electrokinetic coupling in unsaturated porous media: Journal of Colloid and Interface Science, **313**, 315–327, doi: 10.1016/j.jcis.2007.03.037.
Revil, A., V. Naudet, J. Nouzaret, and M. Pessel, 2003, Principles of electrography applied to self-potential electrokinetic sources and hydrogeological applications: Water Resources Research, **39**, 1114, doi: 10.1029/2001WR000916.
Revil, A., H. Schwaeger, L. M. Cathles, and P. Manhardt, 1999, Streaming potential in porous media. 2. Theory and application to geothermal systems: Journal of Geophysical Research, **104**, no. B9, 20033–20048.
Roden, J. A., and S. D. Gedney, 2000, Convolution PML, (CPML): An efficient FDTD implement of CFS-PML for arbitary media: Microwave and Optical Technology Letters, **27**, 334–339.
Sen, M., and P. L. Stoffa, 1995, Global optimization methods in geophysical inversion: Advances in Exploration Geophysics: Elsevier Science Publ. Co., Inc..
Stern, O., 1924, Zur Theorie der elektrolytischen Doppelschicht (The theory of the electrolytic double shift): Zeitschrift Fur Elektrochemie Und Angewandte Physikalische Chemie, **30**, 508–516.
Sternberg, B. K., 1979, Electrical resistivity of the crust in the southern extension of the Canadian shield-layered earth models: Journal of Geophysical Research, **84**, 212–228.
Strahser, M. H. P., W. Rabbel, and F. Schildknecht, 2007, Polarization and slowness of seismoelectric signals, a case study: Near Surface Geophysics, **5**, 97–114.
Suski, B., A. Revil, K. Titov, P. Konosavsky, C. Dagès, M. Voltz, and O. Huttel, 2006, Monitoring of an infiltration experiment using the self-potential method: Water Resources Research, **42**, W08418, doi: 10.1029/2005WR004840.
Tarantola, A., 2005, Inverse Problem Theory. Methods for model parameter estimation: Society of Industrial and Applied Mathematics.
Thompson, A. H., and G. A. Gist, 1993, Geophysical applications of electrokinetic conversion: The Leading Edge, **12**, 1169–1173.
Thompson, A. H., S. Hornbostel, J. Burns, T. Murray, R. Raschke, J. Wride, P. McCammon, J. Sumner, G. Haake, M. Bixby, W. Ross, B. White, M. Zhou, and P. Peczak, 2007, Field tests of electroseismic hydrocarbon detection: Geophysics, **72**, no. 1, N1–N9.
Zeng, Y. Q., J. Q. He, and Q. H. Liu, 2001, The application of the perfectly matched layer in numerical modeling of wave propagation in poroelastic media: Geophysics, **66**, 1258–1266.
Zeng, Y. Q., and Q. H. Liu, 2001, A staggered-grid finite-difference method with perfectly matched layers for poroelastic wave equations: Journal of the Acoustical Society of America, **109**, no. 6, 2571–2580.